Insights into the surface and redox properties of single-walled carbon nanotube—cobalt(II) tetra-aminophthalocyanine self-assembled on gold electrode

Kenneth I. Ozoemena[a, 1], Tebello Nyokong[b, 1], Duduzile Nkosi[a], Isabelle Chambrier[c] and Michael J. Cook[c]

[a]Chemistry Department, **University of Pretoria**, Pretoria 0002, South Africa
[b]Chemistry Department, Rhodes University, Grahamstown 6140, South Africa
[c]School of Chemical Sciences and Pharmacy, University of East Anglia, Norwich, Norfolk NR4 7TJ, United Kingdom

Abstract

This paper describes for the first time the electrochemical properties of redox-active self-assembled films of single-walled carbon nanotubes (SWCNTs) coordinated to cobalt(II)tetra-aminophthalocyanine (CoTAPc) by sequential self-assembly onto a preformed aminoethanethiol (AET) self-assembled monolayer (SAM) on a gold electrode. Both redox-active SAMs (Au-AET-SWCNT and Au-AET-SWCNT-CoTAPc) exhibited reversible electrochemistry in aqueous (phosphate buffer) solution. X-ray photoelectron spectroscopy (XPS) confirmed the appearance on the gold surface of the various elements found on the SAMs. Atomic force microscopy (AFM) images prove, corroborating the estimated electrochemical surface concentrations, that these SAMs lie normal to the gold surface. Electrochemical impedance spectroscopy (EIS) analyses in the presence of $[Fe(CN)_6]^{3-/4-}$ as a redox probe revealed that the Au-AET-SWCNT-CoTAPc showed much lower ($\sim$10 times) electron-transfer resistance (R_{et}) and much higher ($\sim$10 times) apparent electron-transfer rate constant (k_{app}) compared to the Au-AET-SWCNT SAM. Interestingly, a preliminary electrocatalytic investigation showed that both SAMs exhibit comparable electrocatalytic responses towards the detection of

dopamine in pH 7.4 phosphate buffer solutions (PBS). The electrochemical studies (cyclic voltammetry (CV) and EIS) prove that SWCNT greatly improves the electronic communication between CoTAPc and the Au electrode surface.

Article Outline

1. Introduction

The transition metallophthalocyanine (MPc) complexes have shown themselves as versatile macrocyclic organometallic complexes with applications in several technologically relevant areas [1], [2] and [3], notably in the design and fabrication of electrochemical sensors where their use has escalated over the last two decades because of their excellent physico-chemical, electronic and electrocatalytic properties [4], [5] and [6]. Like the MPc complexes, carbon nanotubes (CNTs), single-walled carbon nanotubes (SWCNTs) or multi-walled (MWCNTs), exhibit unique physico-chemical and electronic properties ideal for constructing efficient electrochemical sensors [7], [8], [9], [10] and [11]. Thus, rational integration of these two remarkable π-electron species may

revolutionize their applications in a plethora of areas, especially in electrocatalysis and nanofabrication of molecular electronic and sensing devices. Without doubt, most of the potential applications of MPc and CNTs in electronic, photoconductive and heterogeneous electrocatalysis and sensing devices will require their use as thin films. Self-assembly represents a more efficient technique for fabricating electrodes based on CNT [8], [12] and [13] or MPc [14], [15], [16], [17], [18], [19] and [20] thin films compared to such other thin film formation methodologies such as drop-dry and spin coating.

Self-assembly may simply be described as a spontaneous, coordinated chemical reaction of individual molecular building blocks (especially alkanethiols and thiol-derivatised organomolecules) to create stable, well-organized arrays of ultrathin superstructure films on coinage metals, notably gold [21], [22], [23], [24], [25] and [26]. The formation of self-assembled monolayers (SAMs) of organomolecules on gold surfaces has continued to attract considerable research interests due to their crucial importance in biology, chemistry and supramolecular nanotechnology. SAMs have been known to offer convenient model systems for probing the interfacial electron-transfer processes [24], [25], [26] and [27], and have been extensively studied in corrosion protection [24], [25], [26], [28] and [29], fabrication of electrochemical- and bio-sensors [15], [17], [18], [19], [20], [30], [31], [32] and [33] and molecular electronic devices [34] and [35].

Few reports [36], [37], [38], [39] and [40] have described the integration of CNT with MPc complexes, especially for sensor development [38], [39] and [40], however, until now no research group has addressed the fabrication of CNT-MPc SAMs nor their electron transport (redox) properties. In this work, we describe the first example of a self-assembled SWCNT tethered to cobalt(II)tetra-aminophthalocyanine (CoTAPc) complex (Scheme 1). There have been reports on the SAMs on CNT, especially with the SWCNT, integrated with molecules of biological [8], [9] and [10] and chemical [11] and [41] interests, but not with any MPc complex.

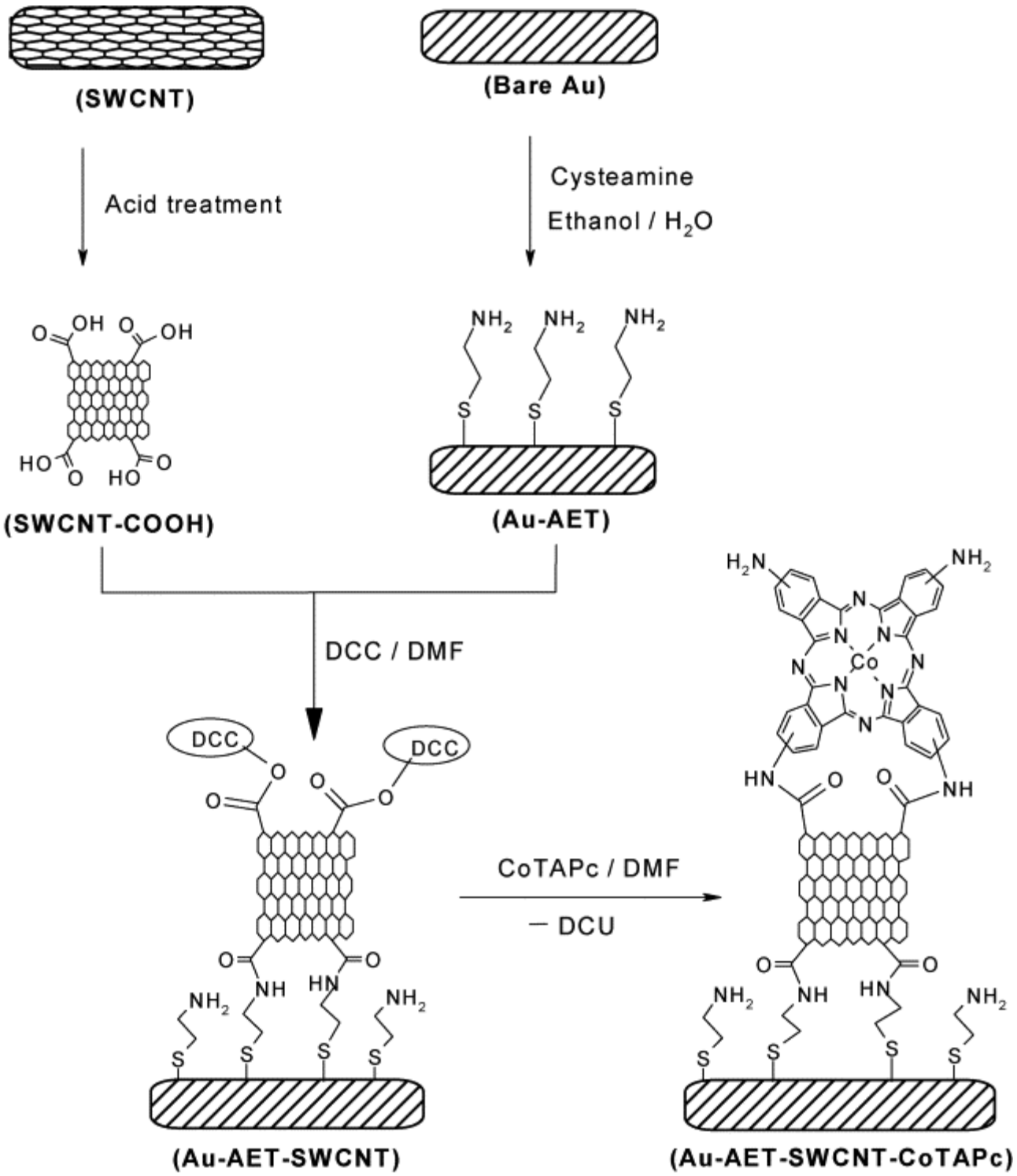

Scheme 1. Schematic representation of the self-assembly processes of the SWCNT and SWCNT-CoTAPc on a gold electrode.

When the molecular building blocks for SAMs are redox-active, as in this work, electrochemical techniques (notably cyclic voltammetry (CV) and electrochemical impedance spectroscopy (EIS)) unlike other surface techniques provide more powerful insights into the surface coverage of the individual components, their adsorption strengths, chemical reactivities with redox probes and redox-active analytes, etc. [17], [18], [19], [20], [25], [42], [43], [44], [45] and [46]. Hence, in this work, we employed CV and EIS to demonstrate that the redox-active CoTAPc can be electrically connected to the gold electrode surface via SWCNTs, which act as efficient conductive electrical nanowires. Also, this study is part of our attempts to provide simpler strategies for making MPc-based SAMs using easy-to-make MPc complexes (such as the MTAPc) rather than the thiol-derivatized MPc complexes. Sulphur-containing MPc complexes rank among the least reported in the literature as their synthesis is time-consuming, costly and difficult and yet less stable than MTAPc complexes.

2. Experimental

2.1. Materials and reagents

Aminoethanethiol (cysteamine) hydrochloride (AET) was obtained from Sigma. Dicyclohexylcarbodiimide (DCC) used as condensing agent and single-walled carbon nanotubes were obtained from Aldrich. Cobalt tetra-aminophthalocyanine complex was synthesized and characterized according to established procedures [47], [48] and [49]. Dopamine hydrochloride was obtained from Sigma. *N*,*N*-dimethylformamide (DMF) was obtained from Sigma–Aldrich, and was distilled and dried before use. Ultra pure water of resistivity 18.2 MΩ was obtained from a Milli-Q Water System (Millipore Corp., Bedford, MA, USA) and was used throughout for the preparation of solutions. Phosphate buffer solutions (PBS) at various pHs were prepared with appropriate amounts of K_2HPO_4 and KH_2PO_4, and the pH adjusted with 0.01 M H_3PO_4 or NaOH. All electrochemical experiments were performed with nitrogen-saturated PBS. All other reagents were of analytical grade and were used as received from the suppliers without further purification.

2.2. Apparatus and procedure

All electrochemical experiments were carried out using an Autolab potentiostat PGSTAT 302 (Eco Chemie, Utrecht, The Netherlands) driven by the General Purpose Electrochemical Systems data processing software (GPES, software version 4.9). Square wave parameters were: step potential 5 mV; equilibration time 5 s, amplitude 25 mV at a frequency of 15 Hz. The working electrode was bare gold (r = 0.8 mm, BAS) or the same gold electrode modified with the investigated SAMs. A Ag|AgCl wire and platinum wire were used as pseudo-reference and counter electrodes, respectively. Electrochemical impedance spectroscopy measurements were performed with an Autolab FRA software between 1.0 Hz and 10 kHz using a 5 mV rms sinusoidal modulation in a solution of 1 mM of $K_4Fe(CN)_6$ and 1 mM $K_3Fe(CN)_6$ (1:1) mixture containing 0.1 M KCl, and at the $E_{1/2}$ of the $[Fe(CN)_6]^{3-/4-}$ (0.13 V versus Ag|AgCl). A non-linear least squares (NNLS) method based on the EQUIVCRT programme [50] was used for automatic fitting of the obtained EIS data. All experiments were performed at 25 ± 1 °C. Solutions were deaerated by bubbling nitrogen prior to the experiments and the electrochemical cell was kept under a nitrogen atmosphere throughout the experiments.

2.3. Preparation of self-assembled SWCNT-CoTAPc film

Scheme 1 shows the self-assembly strategy employed in the preparation of the various SAMs onto gold surfaces (Au-AET, Au-AET-SWCNT and Au-AET-SWCNT-CoTAPc). The purification and chemical shortening of the SWCNTs to uncapped nanotubes bearing acidic functions (SWCNT-COOH) were carried out following the established multi-step oxidative acidic digestion procedures [8], [51] and [52]. The gold electrode used for the SAM was first cleaned using the usual procedure [12] and [51]. SAMs were obtained by the usual adsorption method from dilute solution of adsorbates [53]. In summary, the bare Au electrode was first polished in an aqueous slurry of alumina (<10 μm) on a SiC-emery paper (type 2400 grit), and then to a mirror finish on a Buehler felt pad. The electrode was then subjected to ultrasonic vibration in absolute ethanol to remove residual alumina particles that might be trapped at the surface. Finally, the electrode was etched for about 2 min in a hot 'Piranha' solution (1:3 (v/v) 30% H_2O_2 and concentrated H_2SO_4) and then rinsed with copious amounts of ultrapure Millipore water followed by ethanol. (Caution:

Piranha solution is known to react violently with organic materials and can explode when stored in closed containers, so it must be handled with caution.) This stage was necessary to remove organic contaminants. The cleanliness of the bare electrode surface was finally established by placing it in 0.5 M H_2SO_4 and scanning the potential between −0.5 and 1.5 V (versus Ag|AgCl wire) at a scan rate of 0.05 V s^{-1} until a reproducible scan was obtained. After this check, the electrode was again rinsed with absolute ethanol and immediately placed into a nitrogen-saturated absolute ethanol solution of AET (50 mg/120 ml) for 8 h at ambient temperature. The Au-AET electrode was thoroughly rinsed in absolute ethanol solution before reacting with SWCNT. A 3 mg SWCNT-COOH was first dispersed in 1 ml pure dry DMF with 0.5 mg DCC to convert the –COOH groups at the ends of the SWCNT into active carbodiimide esters. The surface condensation of the Au-AET electrode was achieved by placing the electrode in the black solution of SWCNT/DCC/DMF for 48 h. Acid-treated SWCNT exhibited good solubility in DMF with no detectable precipitate even after several months, hence making this reaction possible without the need for stirring the deposition solution during long deposition periods. The condensation of the –COOH functional groups of the SWCNT-COOH with the $–NH_2$ groups of the AET SAM resulted in the formation of the amide bonds [8]. To minimize possible experimental errors from the use of different gold electrodes, one electrode was used for all experiments reported in this work. The roughness factor of this gold electrode was first determined, after thorough cleaning as described above, by the conventional methodology [25] and [26] using the Randles-Sevčik equation:

$$I_{pa}=(2.69\times10^5)n^{3/2}AD^{1/2}Cv^{1/2} \quad (1)$$

where n is the number of electrons involved (n = 1 in the $[Fe(CN)_6]^{3-/4-}$ redox system), A is the geometric area of the electrode (0.02011 cm^2), D is the diffusion coefficient of the $[Fe(CN)_6]^{3-}$ = 7.6×10^{-6} cm^2 s^{-1} [30], while $C = 1.0 \times 10^{-6}$ mol cm^{-3} is the used bulk concentration of the $[Fe(CN)_6]^{3-}$. From the slope of the plot of the anodic peak current (I_{pa}) versus the scan rate (v, ranging from 10 to 200 m V s^{-1}), the experimentally determined surface area (A) of 0.02655 cm^2 was obtained leading to a surface roughness factor of 1.32.

The CoTAPc was attached to the free ends of the SWCNT by placing the Au-AET-SWCNT electrode in a DMF solution containing ~1.0×10^{-3} M CoTAPc for 48 h. The surface of the Au-AET-SWCNT electrode is expected to contain some active carbodiimide esters that would be attacked by the amino functional groups of the CoTAPc to generate the SWCNT-CoTAPc via amide bonds with the release of dicyclohexylurea (DCU) in the deposition solution. Similarly, Au-CoTAPc was formed simply by placing the clean gold electrode in DMF solution containing ~1.0×10^{-3} M CoTAPc for 48 h. Upon removal from the deposition solution, prior to electrochemical experiments, the electrode was thoroughly rinsed with ethanol and dried in a nitrogen atmosphere. The modified electrode was conditioned by placing in pH 4.4 phosphate buffer solution and continuously scanning the potential between −0.5 and 0.6 V (versus Ag|AgCl) for the Au-AET and Au-AET-SWCNT and −0.5 and 0.6 V (versus Ag|AgCl) for the Au-AET-SWCNT-CoTAPc at a scan rate of 50 m V s^{-1} until a reproducible scan was obtained. When not in use, the sensor was stored in nitrogen-saturated phosphate buffer solution (pH 4.4). Atomic force microscopy (AFM) images were recorded in the contact mode in air with a MultiMode Nanoscope IV Microscope (Digital Instruments) at a scan rate of 0.50 Hz. Gold-coated microscope glass slides used for immobilizing the SAMs for AFM studies were obtained as described before [54]. Briefly, glass substrates (Glass microscope slides, BDH Ltd.) were first cleaned in an aqueous methanol–potassium hydroxide solution, thoroughly rinsed with copious amount of fresh Millipore water and then placed in a stream of refluxing propan-2-ol and dried in air. The cleaned, dried glass substrates were first coated with a 5 nm layer of chromium (99.999% purity, Johnson Matthey Ltd.) and finally by a 45 nm layer of gold (99.999% purity, Johnson Matthey Ltd.). Both chromium and gold layers were deposited by thermal evaporation under vacuum using an Edwards Auto 306 vacuum evaporator. The SAMs were obtained using the same procedure described in Scheme 1. Prior to use for SAM depositions, the gold-coated glass slides were placed in a Piranha solution for about 5 min, and thoroughly rinsed with Millipore water. The X-ray photoelectron spectra (XPS) were obtained using a Physical Electronics model 5400 spectrometer system with monochromatic Mg Kα radiation at 1253.6 eV. The take-off angle was fixed at 45°. The binding energies (BE) for the peak were referenced to the Au $4f_{7/2}$ at 84.0 eV. As for the

AFM studies, XPS experiments were performed with gold-coated glass slides as substrates for the SAMs.

3. Results and discussion

3.1. XPS and AFM characterisation of the self-assembled films

Fig. 1 shows the comparative survey X-ray photoelectron spectra of the (i) bare; (ii) Au-AET; (iii) Au-AET-SWCNT; and (iv) Au-AET-SWCNT-CoTAPc. The S (2p) peak at 162.5 eV is assigned to the normal gold–sulphur bond [16], [55], [56], [57], [58] and [59].

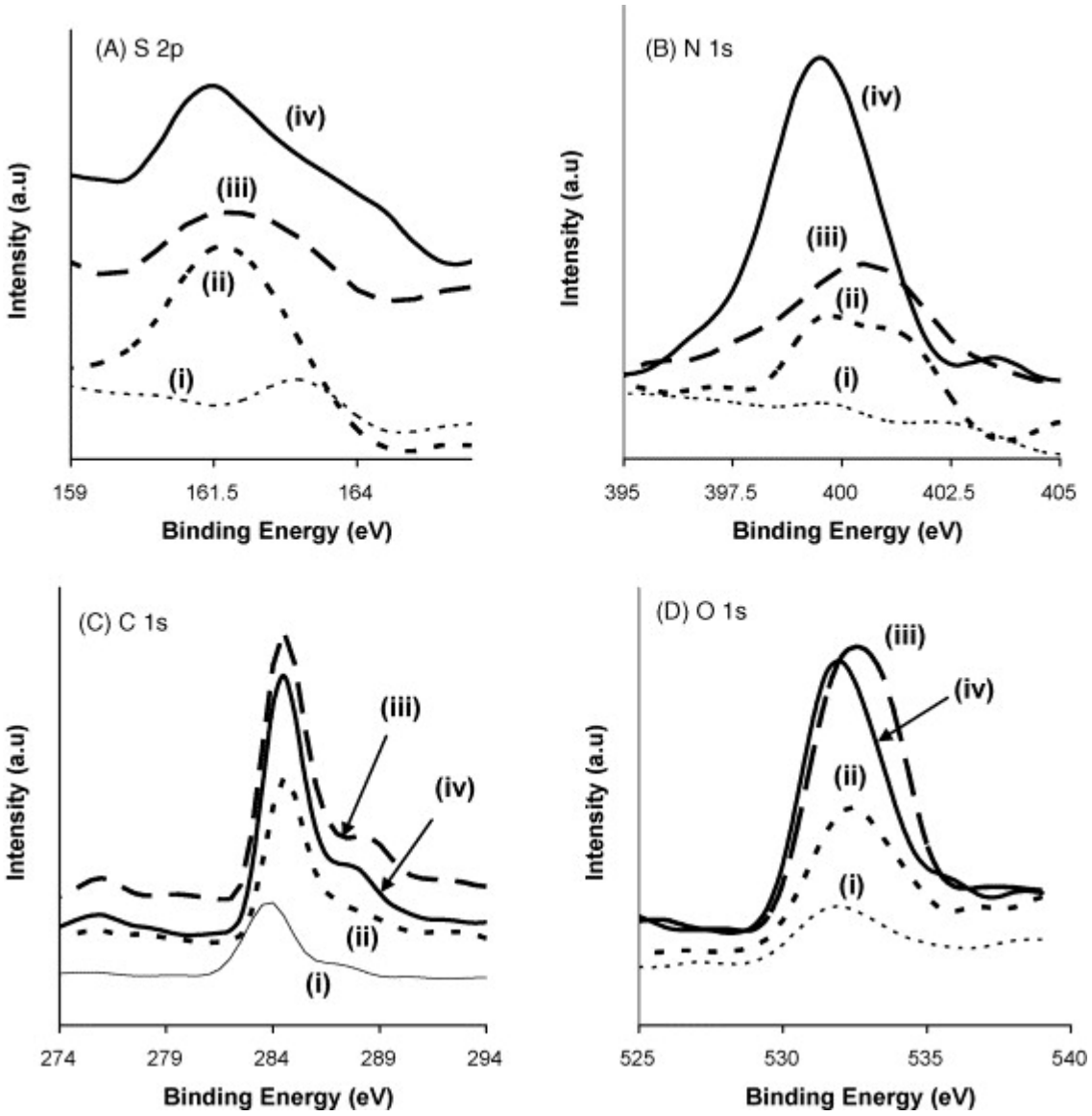

Fig. 1. X-ray photoelectron spectra of (A) sulphur 2p; (B) nitrogen 1s; (C) carbon 1s and (D) oxygen 1s regions of the (i) bare Au; (ii) Au-AET; (iii) Au-AET-SWCNT and (iv) Au-AET-SWCNT-CoTAPc SAMs.

The presence of the N atoms (in the BE region of 395–405 eV) in the SAMs are evident in Fig. 1(B). The cysteamine SAM exhibited two strong components for the N (1s) peak at 399.5 and 401 eV, which is in agreement with literature for cysteamine SAMs [56]. The N (1s) peak for the phthalocyanine is known to occur at either 398 or 400 eV [59], thus the appearance of the N (1s) peak for the CoTAPc at 399.5 eV confirms the attachment of the CoTAPc on the SWCNT. The sharpness and high intensity of this peak

possibly indicates the presence of free or unbound amino groups of the CoTAPc. It is well known [16] that oxygen and carbon are almost always found on putatively bare surfaces due to contaminants (e.g., “adventitious carbon”). Despite this disadvantage, however, the C (1s) and O (1s) peaks observed in the SAMs studied in this work provide some useful information on the carbon and oxygen moieties. As expected, in terms of peak intensity and BE width, SWCNT exhibits high concentrations of carbon and oxygen in the Fig. 1C (iii) and D (iii), respectively. Unlike the cysteamine SAM (Fig. 1C (ii)), the SWCNT (Fig. 1C (iii)) and CoTAPc (Fig. 1C (iv)) SAMs exhibit shoulders in the BE regions of 288 and 289 eV, in excellent agreement with literature values of 288.4 and 289.1 eV for the HN–C═O and HO–C═O groups, respectively [57] and [58], indicative of covalent linkage of nitrogen during self-assembly. Unlike other SAMs, the Au-AET-CNT-CoTAPc exhibited a clearly defined peak at the BE of 783.0 eV (not shown) attributable to Co(II) peak (Co, $2p_{3/2}$) [59].

AFM studies were conducted to give insights into the surface morphologies of the formed AET-SWCNT and AET-SWCNT-CoTAPc SAMs. As exemplified in Fig. 2 for the AET-SWCNT-CoTAPc films, each AFM image clearly proves that the SAM lie perpendicular to the gold surface. AFM image of AET-SWCNT (not shown) gave the same needle-like protrusions, in conformity with literature reports [8]. Such standing position is made possible by covalent bonding [60].

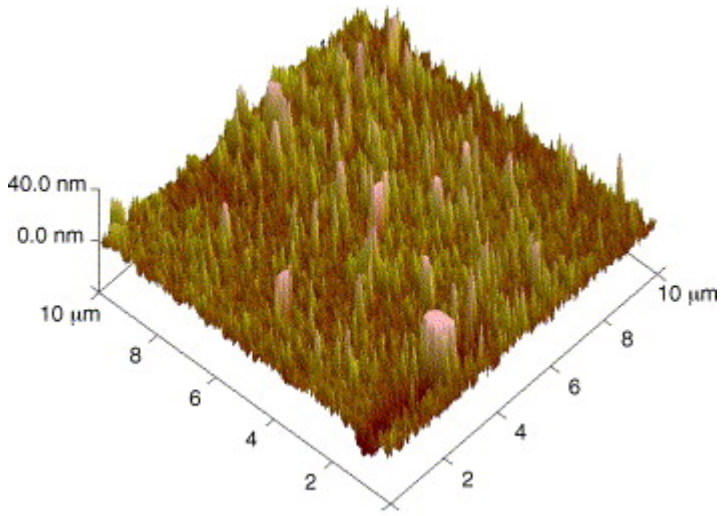

Fig. 2. Typical AFM image of aligned AET-SWCNT-CoTAPc modified gold surface.

3.2. Electrochemical properties of the self-assembled films

We began our electrochemical investigations with repetitive scanning of each of the modified gold electrodes in pH 4.4 phosphate buffer solution until a reproducible scan was obtained. This electrochemical pre-treatment serves to further remove any physically adsorbed species on the surface of the modified electrodes not removed by the rinsing process described in the experimental and, most importantly, to give an insight into the electrochemical stability of these electrodes which is crucial to their studies and application in aqueous solutions. Fig. 3 presents cyclic voltammetric evolutions during 50 repetitive scanning of the Au-AET (A), Au-AET-SWCNT (B) and Au-AET-SWCNT-CoTAPc (C) electrodes.

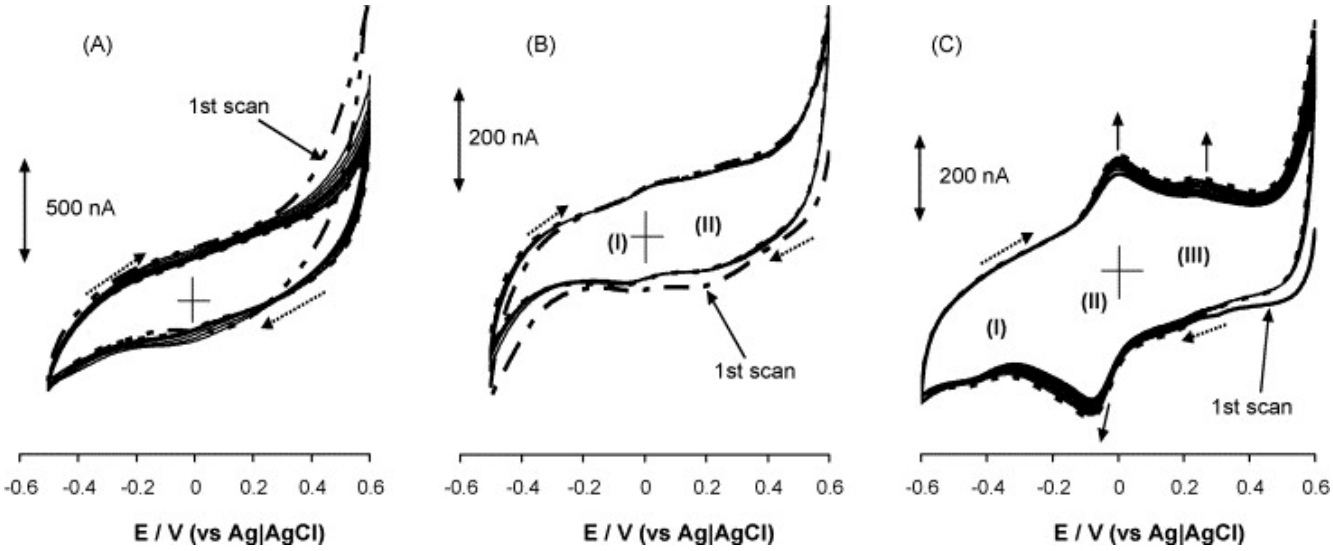

Fig. 3. Cyclic voltammetric profiles of (A) Au-AET; (B) Au-AET-SWCNT and (C) Au-AET-SWCNT-CoTAPc during 20 repetitive scanning in PBS (pH 4.4). Scan rate = 50 mV s^{-1}.

It is evident that these modified electrodes did not show any significant changes between the first and the subsequent scans, confirming their strong electrochemical stability in the aqueous solutions used in this experiment. Similar results were obtained in the pH 7.4 PBS; however pH 4.4 was chosen for the electrode characterisations since it gave relatively better defined redox peaks for the Au-AET-SWCNT and Au-AET-SWCNT-CoTAPc electrodes than pH 7.4. Electrochemical stability is a major attribute of SAM-modified electrodes [21], [22], [23], [24], [25] and [26].

Fig. 4 compares the cyclic voltammograms of bare Au (a), Au-AET (b), Au-AET-SWCNT (c) and Au-AET-SWCNT-CoTAPc in pH 4.4 PBS at a slightly wider window of −0.7 and +0.7 V (versus Ag|AgCl).

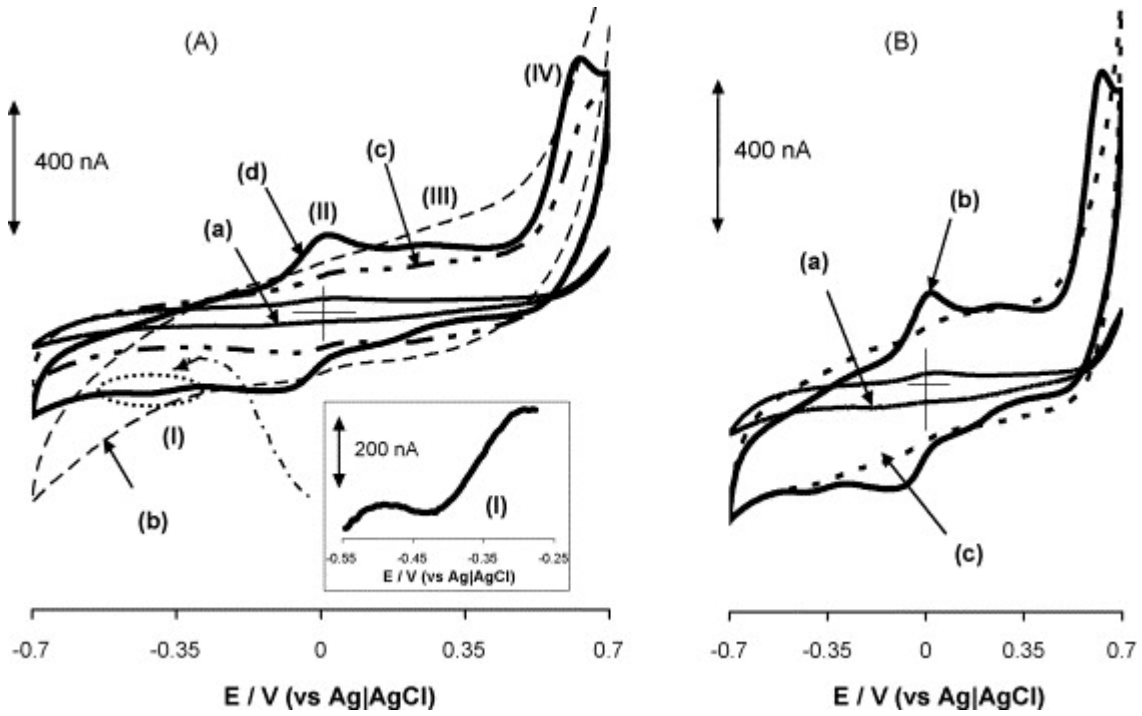

Fig. 4. (A) Comparative cyclic voltammograms of (a) bare Au; (b) Au-AET; (c) Au-AET-SWCNT and (d) Au-AET-SWCNT-CoTAPc in PBS (pH 4.4). (B) Comparative cyclic voltammograms of (a) bare Au; (b) Au-AET-SWCNT-CoTAPc and (c) Au-CoTAPc. Scan rate = 50 mV s^{-1}.

The modification of the Au with any of the species resulted in increased capacitive charging current of the bare gold electrode. Such behaviour is characteristic of SAMs with hydrophilic end groups [25], [26] and [53]. Hydrophilic SAMs, unlike hydrophobic (such as the alkanethiols) are known to increase the capacitive currents. General observation in most carbon nanotube-based electrodes is the high capacitive current, thus the lower capacitive current of the Au-AET-SWCNT compared to the Au-AET may be attributed to the higher hydrophilicity of the latter compared to the former, and/or the enhanced suppression of the electrolyte ions from penetration into the compact film following the introduction of the SWCNT onto the AET surface.

The AET-SAM showed very weak redox process around 0.05 V, possibly due to the redox process of the amine moiety. Both AET-SWCNT and AET-SWCNT-CoTAPc SAMs showed some redox couples. SWCNT (Fig. 3B) exhibited reversible couples at (**I**) of anodic-to-cathodic peak currents (I_{pa}/I_{pc}) of approximately one, peak–peak separation (ΔE_p) of approximately 0.10 V (versus Ag|AgCl)) and half-wave potential ($E_{1/2}$) of −0.01 V (versus Ag|AgCl). Also, a weak couple (**II**) was observed for SWCNT at $E_{1/2}$ of 0.23 V (versus Ag|AgCl). Both redox peaks (**I**) and (**II**) are certainly attributable to the intrinsic redox process of the SWCNT [61], originating from the oxygen-containing moieties (e.g., carboxyl, hydroxyl, and quinone-like groups) on the defects and opened caps of the SWCNT [62] and [63]. It is important to note that our present results, as well as those of other works for SWCNT immobilised onto GCE [59] and MWCNT SAMs [13], contradict the notion that CNTs do not display reversible electrochemistry [11]. As proposed by Luo et al. [61], SWCNT-modified GCE displays four-electron transfer reversible redox processes. These four-electron redox processes may explain the appearance of the redox peaks (**I**) and (**II**) (Fig. 3B) for SWCNT thin film observed in this work. The AET-SWCNT-CoTAPc film (Fig. 3C), on the other hand, showed a pair of remarkably well-defined, reversible redox peak at position (**II**) of ΔE_p and $E_{1/2}$ of approximately 0.09 and 0.04 V (versus Ag|AgCl), respectively. Other couples or peaks observed for the AET-SWCNT-CoTAPc are a weak cathodic peak (**I**) (see Fig. 4A inset) of peak potential (E_p) of −0.44 V (versus Ag|AgCl), weak reversible couple (**III**) of ΔE_p and $E_{1/2}$ of approximately 0.11 and 0.21 V (versus Ag|AgCl), respectively; and an irreversible anodic peak (**IV**) at ca. 0.65 V (Figs. 4A and B). From the well-known electrochemical properties of cobalt (II) phthalocyanine complexes [64], [65], [66] and [67] including our previous works [38], [39] and [40], we can easily assign the redox processes **II** and **IV** of the SWCNT-CoTAPc to the ring processes Pc^{2-}/Pc^{3-} and Pc^{2-}/Pc^{1-}, respectively, while processes **I** and **III** are due to the central cobalt redox processes Co^{II}/Co^{I} and Co^{III}/Co^{II}, respectively. Aside from the covalent bonding depicted in Scheme 1, the π–π interaction between the SWCNT and CoTAPc is also possible. The well-defined reversible electrochemistry of the redox process **II** is an interesting evidence of the interaction between the SWCNT redox process (**I**) and the phthalocyanine ring. Surface-confined, diffusionless species generally give symmetric waves without any peak

separation (i.e., 0 V). The peak separations between the anodic and cathodic peak positions of the AET-SWCNT (**I**) and AET-SWCNT-CoTAPc (**II**) slightly differ from the ideal 0 V expected for surface-confined, diffusionless species. In the present study, however, the peak separation greater than 0 V observed for the SWCNT (**I**) and SWCNT-CoTAPc (**II**) films could point to the kinetic limitations or electrostatic interactions of the molecules in the films.

CoTAPc has been reported to form SAM on gold electrode (Au-CoTAPc) [68] and [69], hence we carried out CV experiments with Au-CoTAPc (Fig. 4B) with a view to investigating the possible influence of the SWCNT on the electrochemistry of Au-AET-SWCNT-CoTAPc SAM. As observed before [67] and clearly corroborated in Fig. 4B (curve c), CoTAPc without SWCNT showed ill-defined CV without any well resolved redox couple, indicative of poor electron-transfer reaction. It is reasonable to conclude from our work that SWCNT markedly improves the electronic communication between CoTAPc and the gold electrode.

The effect of changing scan rates on the CVs of the AET-SWCNT (Fig. 5A) and AET-SWCNT-CoTAPc (Fig. 5B) films gave linear relationships between peak currents versus scan rates, a clear indication of electrochemically stable surface-confined redox-active species. Also, the redox waves shifted to more positive potentials (for anodic) and more negative potentials (for the cathodic); the cathodic wave of the AET-SWCNT-CoTAPc in particular became severely distorted. At the experimental conditions employed in this study, the intrinsic redox couples of the SWCNT were observed at all the investigated scan rates, which also confirms the electrochemical stability of these couples. In general, the peak–peak separation (ΔE) for the Au-AET-SWCNT-CoTAPc was approximately twice that of the Au-AET-SWCNT, a clear indication of faster electron transfer for the latter than the former. This result is the direct consequence of the long distance for electrons to tunnel between the CoTAPc and the Au in comparison to the distance between the SWCNT and the Au. Also, we could attribute such weak electron-transfer processes to enhanced complications of the overlapped redox reactions between the SWCNT and CoTAPc.

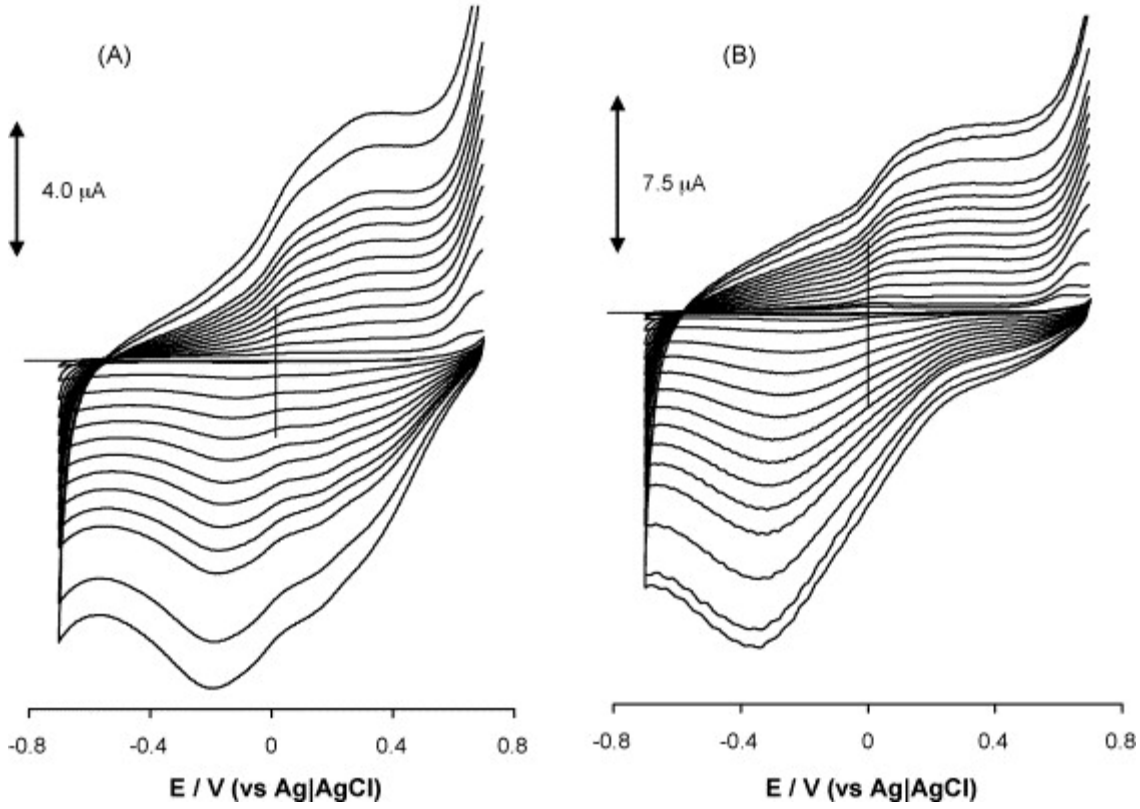

Fig. 5. Effect of varying scan rates (25–1500 mV s^{-1}, inner to outer) of (A) Au-AET-SWCNT and (B) Au-AET-SWCNT-CoTAPc in PBS (pH 4.4).

The surface concentrations (Γ_{SAM}/mol cm^{-2}) of the electrochemically conditioned AET-SWCNT and AET-SWCNT-CoTAPc based films were estimated from the background-corrected charges, Q, under the anodic peaks (**I** for Au-AET-SWCNT and **II** for Au-AET-SWCNT-CoTAPc) using the conventional relationship involving the Faraday constant F (96485 °C mol^{-1}) (Eq. (1)) [25] and [26]:

$$\Gamma_{SAM} = \frac{Q}{nFA} \tag{2}$$

Assuming $n \approx 4$ for SWCNT redox wave [59] and $n = 1$ for the CoTAPc, the surface coverages were estimated as 1.1×10^{-10} mol cm^{-2} ($\sim$$6.6 \times 10^{13}$ particles $cm^{-2} \approx 150$ $Å^2$ per particle) for the Au-AET-SWCNT, and 6.8×10^{-10} mol cm^{-2} ($\sim$ 4.1×10^{14} molecules cm^{-2} or $\sim$24 $Å^2$ per molecule) for the Au-AET-SWCNT-CoTAPc. The values are of similar magnitudes as those reported in the literature for

perpendicularly oriented SAMs of Au-AET-SWCNT [10] and CoTAPc [68] and [69] obtained at long deposition times ≥12 h as carried out in this work. If each CoTAPc molecule assumes flat orientation on the SWCNT surface yielding an area close to 200 $Å^2$ [67], [68], [69] and [70], the coverage should work out to be approximately 1.0×10^{-10} mol cm^{-2}. Thus, the high surface coverage for the CoTAPc is a clear indication of a perpendicular orientation for the CoTAPc. Interestingly, CoTAPc is also known to prefer perpendicular orientation when adsorbed on a gold surface as a SAM [68] and [69]. Also, the cross sectional area for a single SWCNT of diameter of ~1.3 nm [10] should be ~1.33×10^{-14} cm^{-2}, meaning that each SWCNT particle occupies an area of ~133 $Å^2$, which is in close agreement with the surface coverage (~150 $Å^2$) obtained in this work. This result is consistent with the AFM results which showed that these SAMs lie normal to the gold surface.

Further electrochemical properties of the modified electrodes were interrogated in 0.1 M KCl containing the $[Fe(CN)_6]^{3-/4-}$ redox probe. Fig. 6 shows comparative CVs for the bare Au before and after modification with the SAMs of AET, CoTAPc, AET-SWCNT and AET-SWCNT-CoTAPc films.

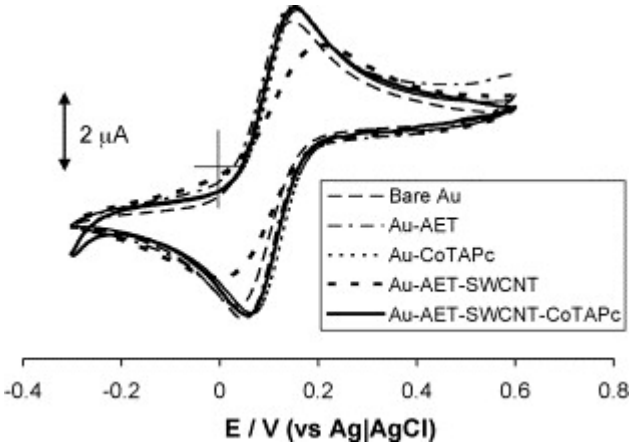

Fig. 6. Comparative cyclic voltammetric profiles of $[Fe(CN)_6]^{3-/4-}$ using the different electrodes. Scan rate = 25 mV s^{-1}.

The peak separation of the AET-SWCNT film (225 mV versus Ag|AgCl) is twice those of the bare Au and other modifying films (~112 mV versus Ag|AgCl). As also observed by others [71], AET SAM leads to enhanced electrochemical response of the $[Fe(CN)_6]^{3-/4-}$ which is attributable to the electrostatic interaction between the positively

charged AET and the negatively charged $[Fe(CN)_6]^{3-/4-}$ redox probe. As a contrast, the weak electron-transfer response seen at the SWCNT film is due to the repulsive interaction between the negatively charged SWCNT and the $[Fe(CN)_6]^{3-/4-}$ probe. CNT-chemically modified electrodes (CMEs) [62], including CNT-SAMs [13] exhibit similar weak redox response for the $[Fe(CN)_6]^{3-/4-}$ redox probe compared to their bare glassy carbon or gold electrodes. As expected, modification with the positively charged Co^{2+} redox-active centre of the CoTAPc led to more reversibility and slight enhancement of the peak current. It should be noted that the difference in behaviour of the electrodes in aqueous solution (pH 4.4, Fig. 4) and in this redox probe (Fig. 6) is certainly the consequence of presence of redox-active species in different electrolyte conditions.

3.3. Electrochemical impedance spectroscopic investigations

Electrochemical impedance spectroscopy measurements were used to further interrogate the electrochemical kinetics at Au|SAM interfaces and to distinguish between the various mechanisms that govern charge transfer [72] and [73]. At the $E_{1/2}$ (~0.13 versus Ag|AgCl) of the $[Fe(CN)_6]^{3-/4-}$ redox system, the Nyquist plots ($Z_{imaginary}$ versus Z_{real}) (Fig. 7A (a–e)) exhibited the characteristic semicircles at high frequencies and a straight line at low frequencies, corresponding to kinetic and diffusion processes, respectively.

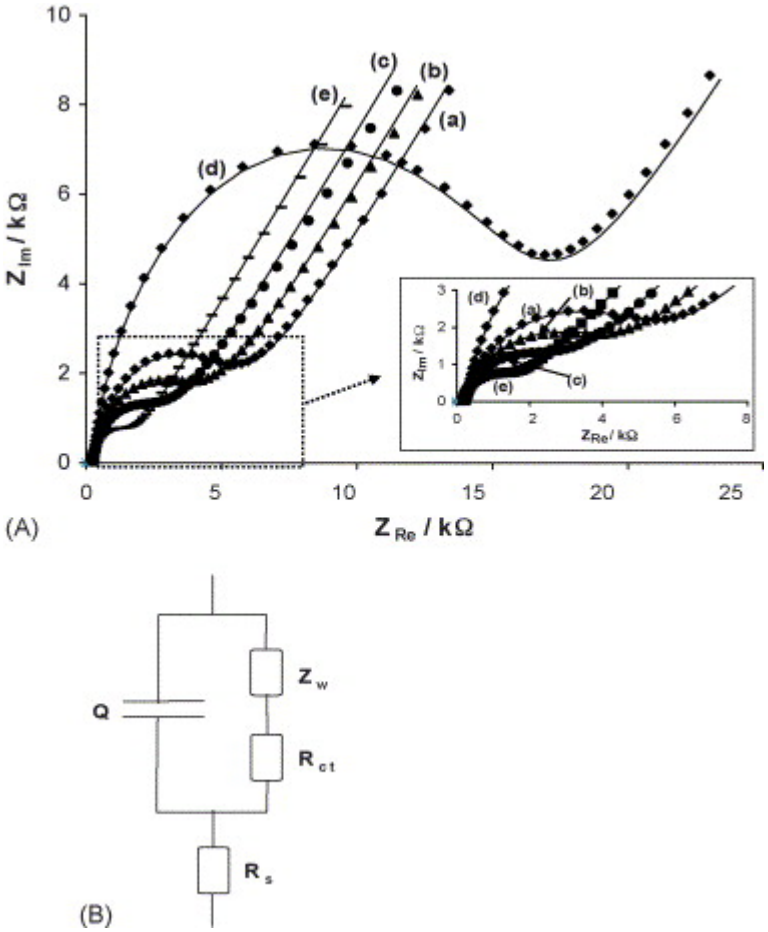

Fig. 7. Typical Nyquist plots resulting from (a) bare Au; (b) Au-AET; (c) Au-CoTAPc; (d) Au-AET-SWCNT and (e) Au-AET-SWCNT-CoTAPc in 0.1 KCl containing equimolar mixture of $K_4Fe(CN)_6$ and $K_3Fe(CN)_6$. Inset (A) shows Nyquist plots at the high frequencies. (B) shows the proposed Randle's model. Applied potential = 0.13 V (vs. Ag|AgCl).

To fit the EIS data at this potential, the spectra were modeled using the Randles' equivalent circuit of mixed kinetic and diffusion control shown in Fig. 7B, where R_s is the resistance of the electrolyte, Q is the membrane capacitance, R_{et} is the electron-transfer resistance (domain of kinetic control) and Z_w is the Warburg impedance (domain of mass transport control) resulting from the diffusion of ions to the electrode interface from the bulk of the electrolyte. As evident in the Nyquist plots, the simulated plots based on the model agree well with the experimental results. Table 1 presents a summary of the estimated EIS parameters for the Randles' model. The Z_w values are about the same for

all the electrodes. Ideally, R_s and Z_w should not be affected by modification of the electrode surface [74].

Table 1.

Summary of estimated EIS parameters obtained for the electrodes at applied potential of 0.13 V (vs. Ag|AgCl)

Electrodes	R_s **(Ω)**	R_{et} **(kΩ)**	Q **(μF)**	Z_w **(Ω $s^{-1/2}$)**	n	k_{app} **(cm s^{-1})**
Bare Au	264.80	5.01	3.74	1.07×10^{-4}	0.90	2.00×10^{-3}
Au-CoTAPc	205.60	2.70	2.70	1.03×10^{-4}	0.86	3.71×10^{-3}
Au-AET	221.01	3.96	2.70	1.07×10^{-4}	0.86	2.53×10^{-3}
Au-AET-SWCNT	236.71	15.40	3.20	1.09×10^{-4}	0.90	0.65×10^{-3}
Au-AET-SWCNT-CoTAPc	170.20	1.38	3.70	1.09×10^{-4}	0.91	7.27×10^{-3}

All experiments were performed at least six times with each of five SAMs obtained at different days using the same gold electrode (errors ≤ 0.3%).

The decrease in R_s (in the 11–36% range) observed on the modified Au is not fully understood at this time but demonstrates that the ohmic resistance of the solution was slightly affected by these films. The Q-value for the bare Au did decrease slightly on modification. The n-values are approximately 0.9, and being <1.0 suggests that the electrodes are not true capacitors. The apparent electron-transfer rate constant k_{app} was obtained from the conventional equation [42]:

$$k_{app} = \frac{RT}{F^2 R_{et} C} \tag{3}$$

where C is the concentration of the $[Fe(CN)_6]^{3-}$ (in mol cm^{-3}, the concentration of $[Fe(CN)_6]^{3-}$ and $[Fe(CN)_6]^{4-}$ are equal), R, T and F have their usual meanings. As reflected in their R_{et} and k_{app} values, the Au-AET-SWCNT-CoTAPc electrode exhibited much faster electron-transfer processes towards $[Fe(CN)_6]^{3-/4-}$ compared to other

electrodes investigated in this work. The data corroborate the CV results shown in Fig. 6 and our explanation thereof. The Bode plots of phase angle versus log *f* (Fig. 8) showed well-defined symmetrical peaks at different maxima.

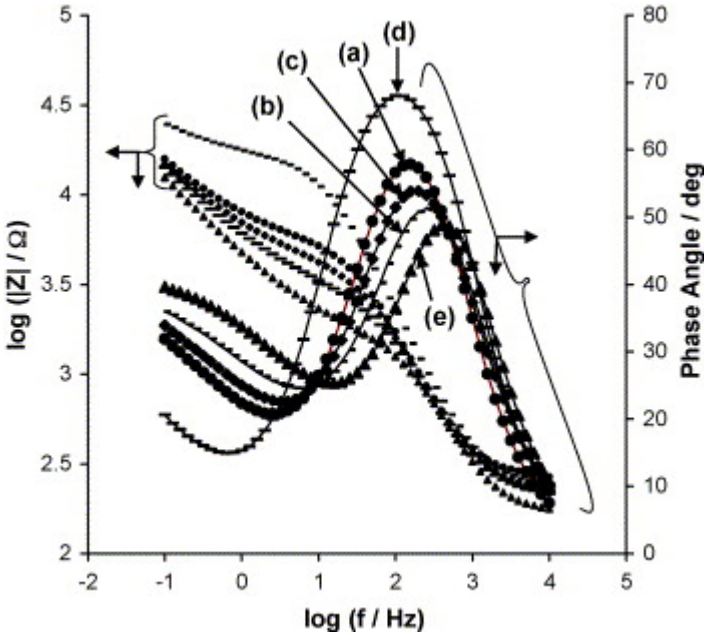

Fig. 8. Typical Bode plots resulting from (a) bare Au; (b) Au-AET; (c) Au-CoTAPc; (d) Au-AET-SWCNT and (e) Au-AET-SWCNT-CoTAPc in 0.1 KCl containing an equimolar mixture of $K_4Fe(CN)_6$ and $K_3Fe(CN)_6$. Applied potential = 0.13 V (vs. Ag|AgCl).

The bare Au gave a maximum value of ≈58° at 126 Hz corresponding to the relaxation process of the Au|solution interface. This relaxation process shifts to different phase angles (ca. 49–68° range) and at lower frequencies (100–398 Hz range) upon modification of the Au, confirming that the $[Fe(CN)_6]^{3-/4-}$ redox reactions now take place at the surface of the modifying films rather than directly on the bare Au surface. The estimated slopes of the Bode plots (log |*Z*| versus log *f*) (Fig. 8), approximately in the −0.6 to −0.7 range, confirm that the Au-SAMs studied in the work are redox-active and are not true capacitors as the estimated slopes are far from the ideal minus one value expected for true capacitors and usually observed for electro-inactive SAMs of alkanethiols.

3.4. Potential electrocatalytic application

Dopamine is a well-known neurotransmitter that has received wide analytical investigations with different modified electrodes. Rather than in-depth analytical investigations, we chose this biologically important probe simply to compare the electrocatalytic response profiles of the modified Au electrodes. As seen in Fig. 9, the anodic oxidation of dopamine in pH 7.4 PBS occurred at 0.30, 0.27, 0.22, 0.15 and 0.17 V (versus Ag|AgCl) at the bare Au (a), Au-CoTAPc (b), Au-AET (c), Au-AET-SWCNT (d) and Au-AET-SWCNT-CoTAPc (e) electrodes, respectively.

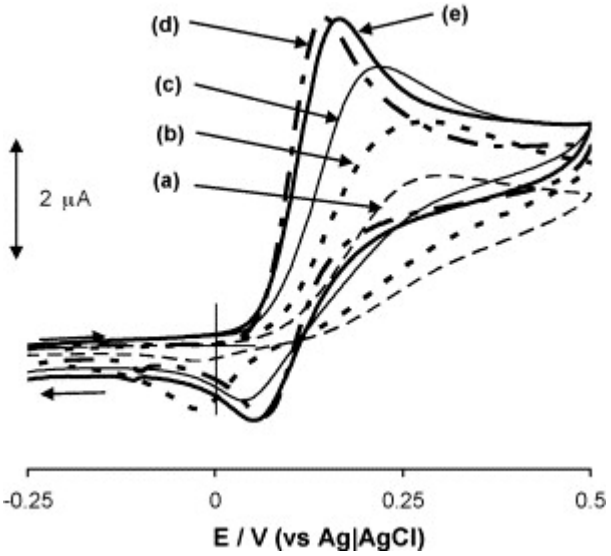

Fig. 9. Comparative cyclic voltammetric profiles for 0.5 mM dopamine in PBS (pH 7.4) at different electrodes; (a) bare Au; (b) Au-CoTAPc; (c) Au-AET; (d) Au-AET-SWCNT and (e) Au-AET-SWCNT-CoTAPc. Scan rate = 50 mV s^{-1}.

The voltammetric evolutions are typical of a dielectronic–diprotonic redox process for dopamine at chemically modified electrodes [75]. Both Au-AET-SWCNT and Au-AET-SWCNT electrodes exhibited a catalytic response (enhanced current at less positive potential) compared to Au-AET and bare Au for this analyte. These results may be rationalized as follows. Dopamine (DAH^+) is protonated (pK_a 8.9) [71] in the buffer solution employed in this study. Since the AET SAM is known [70] to be positively charged at ≤pH 7.6, then the relatively more positive anodic oxidation peak potential (E_{pa} ~ 0.22 V) compared to the SAMs of AET-SWNT (E_{pa} ~ 0.15 V) and AET-SWCNT-CoTAPc (E_{pa} ~ 0.17 V) is due to electrostatic repulsion between the Au-AET

and DAH^+. The improved response of the positively charged Au-AET over the bare Au for the DAH^+ is somewhat surprising. We may attribute this result to possible penetration of the DAH^+ into the AET film as a result of the pinholes created by the repulsive interactions between neighbouring positively charged AET species on the Au surface. If we compare the positions of the Au-CoTAPc (b) and Au-AET-SWCNT-CoTAPc (e) in Fig. 9, it is clear that the CoTAPc activity towards the anodic oxidation of DAH^+ can be improved only in the presence of SWCNT. The electrocatalysis of DAH^+ at the AET-SWCNT-CoTAPc is not surprising as the ability for the redox-active CoPc complexes to electrocatalyze dopamine and its related complexes is well documented [6]. The slightly enhanced catalytic E_{pa} (20 mV) obtained for the AET-SWNT in comparison to the AET-SWCNT-CoTAPc SAM is possibly due to electrostatic attraction between the negatively charged Au-AET-SWCNT and DAH^+. In general, the data obtained here clearly indicate that SWCNT greatly improves the electronic communication between the dopamine and the bare Au. Plot of anodic peak current (I_{pa}) against the square root of scan rate ($v^{1/2}$) (for scan rates less than 300 mV s^{-1}, figure not shown) resulted in a straight line, an indication of a diffusion controlled dopamine oxidation. Further studies on the electrocatalytic behaviour of these SAM-based electrodes towards the detection of other biomolecules as well as their mechanistic investigations are underway and will be reported elsewhere.

3.5. Proposed electron-transfer mechanism

As clearly evident from this report (notably the R_{et} values in Table 1, and comparative reponses of the CoTAPc and SWCNT-CoTAPc towards the detection of dopamine in Fig. 9), SWCNT enhances the electronic communication between CoTAPc and the Au electrode surface. The plausible overall charge transfer process at the Au-AET-SWCNT-CoTAPc electrode is hypothesized as schematically represented in Scheme 2, wherein electron transfer consists of four steps (using anodic oxidation process as an example): (1) electron-tunneling from SWCNT to gold; (2) electron transport occurring within SWCNTs; (3) electron-tunneling from the CoTAPc ring and/or central cobalt; and (4) heterogeneous electron transfer between the central cobalt of the CoTAPc and a redox probe (such as the $[Fe(CN)_6]^{3-}/[Fe(CN)_6]^{4-}$) or an analyte (e.g., dopamine).

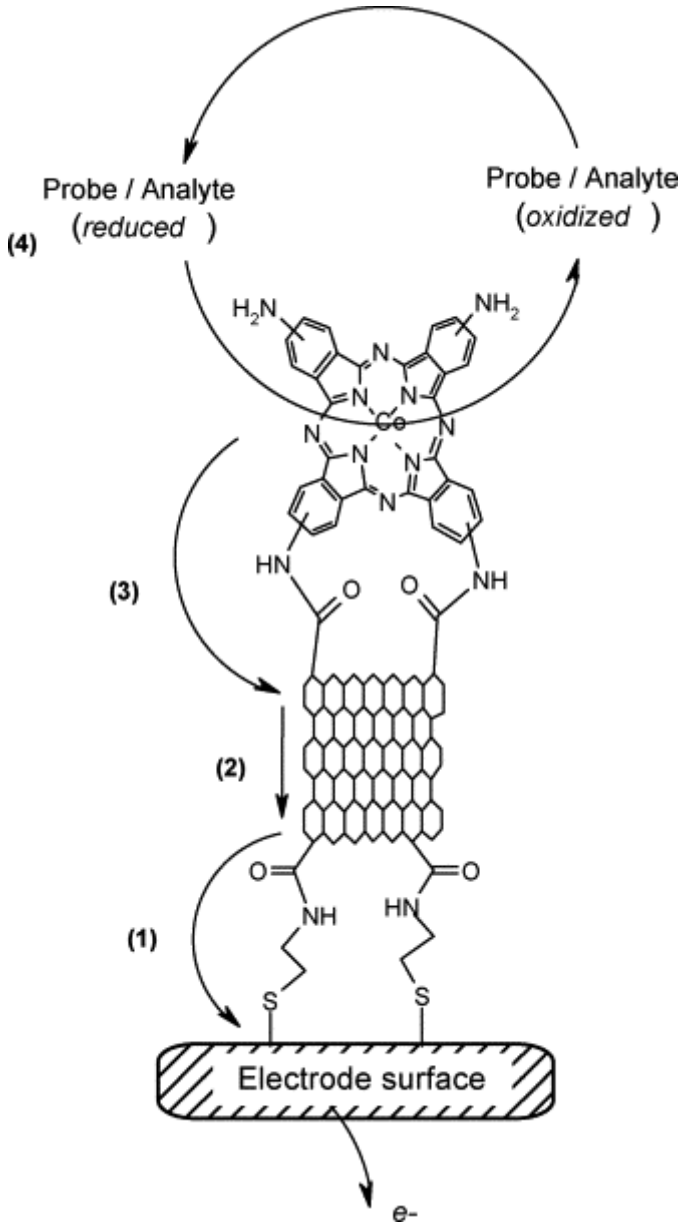

Scheme 2. Schematic representation of electron-transfer processes at Au-AET-SWCNT-CoTAPc SAM electrode (using anodic process as an example). Direction of electron flow is depicted by the arrows. The broken semi-circular arrow (step 4) depicts reversibility of redox probe such as the $[Fe(CN)_6]^{3-/4-}$, while the full semi-circular arrow alone depicts irreversible anodic oxidation for such analyte as dopamine.

As previously proposed for aminothiol SAMs (Au-aminoundecanethiol) [12], through-space tunneling is most likely the possible electron-transfer mechanism for Au-AET. The 'cutting' process of harsh acid-treatment adopted for SWCNT may generate local traps for charge transport, however, it is well documented that the high conductivity of the

immobilized SWCNTs is sufficient enough to make SWCNTs act as efficient conductive nanowires rather than charge traps [11] and [12]. Through-bond tunneling is the electron-transfer mechanism that operates for Au-SAM-redox centers [25], [26] and [76]. Such through-bond process is easily established by reversible cyclic voltammetric plots, indicating that such redox centers can easily exchange electron with the underlying electrode surface vial tunneling [25], [26], [76], [77] and [78]. Thus, we can reasonably assume that efficient through-bond tunneling takes place between redox-active CoTAPc and gold at the Au-AET-SWCNT-CoTAPc electrode. Facile heterogeneous electron transfer has been known to occur between immobilized carbon nanotubes as well as transition metallophthalocyanine complexes. Thus, steps 1–4 can be well understood.

4. Conclusion

We have shown in this work the electrochemical properties of redox-active self-assembled films of single-walled carbon nanotube coordinated to cobalt(II)tetra-aminophthalocyanine by sequential self-assembly onto a preformed aminoethanethiol self-assembled monolayer on a gold electrode. Cyclic voltammetric and impedance spectroscopic characteristics of the redox-active SAMs revealed reversible electrochemistry in aqueous solutions with different electron-transfer rates. SWCNT greatly improves the electronic communication between CoTAPc and the Au electrode surface. A preliminary electrocatalytic investigation proved that both SAMs exhibit comparable electrocatalytic responses towards the detection of dopamine in pH 7.4 PBS. This proposed electrode fabrication technique is unique; it can be used for fundamental studies of the electron-transfer processes of surface-confined metalloporphyrin and metallophthalocyanine complexes and, importantly, it promises to provide an opportunity for controlled fabrication of stable organometallic sensing platforms. For example, further studies to explore other electrocatalytic properties (e.g., influence of surface charges to electron transfer) and sensing capabilities of this type of MPc-SAM to organic analytes will constitute some of the subjects of our future investigations.

References

[1] In: C.C. Leznoff and A.B.P. Lever, Editors, *Phthalocyanines: Properties and Applications* **vol. 1–4**, VCH publishers, New York (1989–1996).

[2] N.B. McKeown, Phthalocyanine Materials: Synthesis, Structure and Function, Cambridge University Press, Cambridge (1998).

[3] In: K.M. Kadish, K.M. Smith and R. Guilard, Editors, *The Porphyrin Handbook* **vol. 15–20**, Academic Press, Boston (2003) (Chapters 97–122).

[4] P. Vasuvedan, N. Poughat and A.K. Shuklat, *Appl. Organomet. Chem.* (1996), p. 591.

[5] T. Nyokong and S. Vilakazi, *Talanta* **61** (2003), p. 27.

[6] K.I. Ozoemena and T. Nyokong In: C.A. Grimes, E.C. Dickey and M.V. Pishko, Editors, *Encyclopedia of Sensors* **vol. 3**, American Scientific Publishers, California (2006), p. 157 (Chapter E, and references therein).

[7] C.E. Banks, R.R. Moore, T.J. Davies and R.G. Compton, *Chem. Commun.* (2004), p. 1804.

[8] J.J. Gooding, R. Wibowo, J. Liu, W. Yang, D. Losic, S. Orbons, F.J. Meams, J.G. Shapter and D.B. Hibbert, *J. Am. Chem. Soc.* **125** (2003), p. 9006.

[9] J.J. Gooding, *Electrochim. Acta* **50** (2005), p. 3049.

[10] F. Patolsky, Y. Weizmann and I. Willner, *Angew. Chem. Int. Ed.* **43** (2004), p. 2113.

[11] L. Sheeney-Haj-Ichia, B. Basnar and I. Willner, *Angew. Chem. Int. Ed.* **44** (2005), p. 78.

[12] P. Diao and Z. Liu, *J. Phys. Chem. B* **109** (2005), p. 20906.

[13] L. Su, F. Gao and L. Mao, *Anal. Chem.* **78** (2006), p. 2651.

[14] M.J. Cook, *Pure Appl. Chem.* **71** (1999), p. 2145.

[15] M.J. Cook, *J. Mater. Chem.* **6** (1996), p. 677.

[16] Z. Li, M. Lieberman and W. Hill, *Langmuir* **17** (2001), p. 4887.

[17] K.I. Ozoemena, T. Nyokong and P. Westbroek, *Electroanalysis* **15** (2003), p. 1762.

[18] K. Ozoemena and T. Nyokong, *Electrochim. Acta* **47** (2002), p. 4035.

[19] K.I. Ozoemena and T. Nyokong, *J. Electroanal. Chem.* **579** (2005), p. 283.

[20] T.R.E. Simpson, D.A. Russell, I. Chambrier, M.J. Cook, A.B. Horn and S.C. Thorpe, *Sens. Actuators B* **29** (1995), p. 353.

[21] R.G. Nuzzo and D.L. Allara, *J. Am. Chem. Soc.* **105** (1983), p. 4481.

[22] C.D. Bain, H.A. Biebuyck and G.M. Whitesides, *Langmuir* **5** (1989), p. 7432.

[23] H.O. Finklea, D.A. Snider, J. Fedyk, E. Sabatani, Y. Gafini and I. Rubinstein, *Langmuir* **9** (1993), p. 3660.

[24] A. Ulman, An Introduction to Ultrathin Organic Films: From Langmuir-Blodgett to Self-assembly, Academic Press, San Diego (1991).

[25] H.O. Finklea In: A.J. Bard and I. Rubinstein, Editors, *Electroanalytical Chemistry* **vol. 19**, Marcel Dekker, New York (1996), p. 109.

[26] H.O. Finklea In: R.A. Meyers, Editor, *Encyclopedia of Analytical Chemistry: Applications, Theory and Instrumentations* **vol. 11**, Wiley, Chichester (2000), p. 10090.

[27] H.C. De Long and D.A. Buttry, *Langmuir* **6** (1990), p. 1319.

[28] F.P. Zamborini, J.K. Campbell and R.M. Crooks, *Langmuir* **14** (1998), p. 640.

[29] S. Ramachandran, B.-I. Tsai, M. Blanco, H. Chen, Y. Tang and W.A. Goodard III, *Langmuir* **12** (1996), p. 6419.

[30] J.J. Gooding, V.G. Praig and E.A.H. Hall, *Anal. Chem.* **70** (1998), p. 2396.

[31] Y. Tian, L. Mao, T. Okajima and T. Ohsaka, *Anal. Chem.* **76** (2004), p. 4162.

[32] R.C. Retna and T. Ohsaka, *J. Electroanal. Chem.* **540** (2003), p. 69.

[33] P.N. Mashazi, K.I. Ozoemena and T. Nyokong, *Electrochim. Acta* **52** (2006), p. 177.

[34] K. Kitagawa, T. Morita and S. Kimura, *Langmuir* **21** (2005), p. 10624.

[35] J. Chen, M.A. Reed, A.M. Rawlett and J.M. Tour, *Science* **286** (1999), p. 1550.

[36] J.-S. Ye, Y. Wen, De Zhang, H.F. Cui, G.Q. Xu and F.-S. Sheu, *Electroanalysis* **17** (2005), p. 89.

[37] X. Wang, Y. Liu, W. Qiu and D. Zhu, *J. Mater. Chem.* **12** (2002), p. 1636.

[38] M. Siswana, K.I. Ozoemena and T. Nyokong, *Electrochim. Acta* **52** (2006), p. 114.

[39] K.I. Ozoemena, J. Pillay and T. Nyokong, *Electrochem. Commun.* **8** (2006), p. 1391.

[40] J. Pillay and K.I. Ozoemena, *Electrochim. Acta* **52** (2007), p. 3630.

[41] M. Alvaro, C. Aprile, P. Atienzar and H. Garcia, *J. Phys. Chem. B* **109** (2005), p. 7692.

[42] E. Sabatani and I. Rubinstein, *J. Phys. Chem.* **91** (1987), p. 6663.

[43] K. Nishiyama, S.-I. Tahara, Y. Uchida, S. Tanoue and I. Taniguchi, *J. Electroanal. Chem.* **478** (1999), p. 83.

[44] D. Losic, J.G. Shapter and J.J. Gooding, *Langmuir* **17** (2001), p. 3307.

[45] F. Zhao, F. Huang, Q. Yan and B. Zeng, *Microchim. Acta* **150** (2005), p. 179.

[46] X. Lu, M. Li, C. Yang, L. Zhang, Y. Li, L. Jiang, H. Li, L. Jiang, C. Liu and W. Hu, *Langmuir* **22** (2006), p. 3035.

[47] B.N. Achar, G.M. Fohlen and J.A. Parker, *J. Polym. Sci.* **20** (1982), p. 2773.

[48] S.W. Oliver and T.D. Thomas, *Heterocycles* **22** (1984), p. 2047.

[49] B.N. Achar, G.M. Fohlen, J.A. Parker and J. Keshavaya, *Polyhedron* **6** (1987), p. 1463.

[50] B.A. Boukamp, *Solid State Ionics* **20** (1986), p. 31 (Described in the User Manual for the Frequency Response Analyzer (FRA) software, Eco-Chemie B.V. (2001)).

[51] Z.F. Liu, Z.Y. Shen, T. Zhu, S.F. Huo, L.Z. Ying, Z.J. Shi and Z.N. Gu, *Langmuir* **16** (2000), p. 3569.

[52] J. Chen, M.A. Hamon, H. Hu, Y. Chen, A.M. Rao, P.C. Eklund and R.C. Haddon, *Science* **282** (1998), p. 95.

[53] C.E.D. Chidsey and D.N. Loiacono, *Langmuir* **6** (1990), p. 682.

[54] D.J. Revell, I. Chambrier, M.J. Cook and D.A. Russell, *J. Mater. Chem.* **10** (2000), p. 31.

[55] C.-J. Zhong, R.C. Brush, J. Anderegg and M.D. Porter, *Langmuir* **15** (1999), p. 518.

[56] M. Wirde, U. Gelius and L. Nyholm, *Langmuir* **15** (1999), p. 6370.

[57] Z. Chen, K. Kobashi, U. Rauwald, R. Booker, H. Fan, W.-F. Hwang and J.M. Tour, *J. Am. Chem. Soc.* **128** (2006), p. 10568.

[58] J. Chattopadhyay, F. de Jesus Cortez, S. Chakraborty, N.K.H. Slater and W.E. Billups, *Chem. Mater.* **18** (2006), p. 5864.

[59] In: G.E. Muilenberg, Editor, *Handbook of X-Ray Photoelectron Spectroscopy*, Perkin-Elmer Corp., Eden Praire, Minnesota (1979).

[60] A. Profumo, M. Fagnoni, D. Merli, E. Quartarone, S. Protti, D. Dondi and A. Albini, *Anal. Chem.* **78** (2006), p. 4194.

[61] H. Luo, Z. Shi, N. Li, Z. Gu and Q. Zhuang, *Anal. Chem.* **73** (2001), p. 915.

[62] K. Gong, X. Zhu, R. Zhao, S. Xiong, L. Mao and C. Cheng, *Anal. Chem.* **77** (2005), p. 8158.

[63] C. Hu, X. Cheng and S. Hu, *J. Electroanal. Chem.* **586** (2006), p. 77.

[64] A.B.P. Lever, E.R. Milaeva and G. Speier In: C.C. Leznoff and A.B.P. Lever, Editors, *Phthalocyanines: Properties and Applications* **vol. 3**, VCH, New York (1993).
[65] S. Maree and T. Nyokong, *J. Electroanal. Chem.* **492** (2000), p. 120.
[66] S. Griveau, J. Pavez, J.H. Zagal and F. Bedoui, *J. Electroanal. Chem.* **497** (2001), p. 75.
[67] Y.-H. Tse, P. Janda, H. Lam, W.J. Pietro and A.B.P. Lever, *J. Porphyrins Phthalocyanines* **1** (1997), p. 3.
[68] M.P. Somashekarappa and S. Sampath, *Chem. Commun.* (2002), p. 1262.
[69] M.P. Somashekarappa, J. Keshavaya and S. Sampath, *Pure Appl. Chem.* **74** (2002), p. 1609.
[70] N. kobayashi, P. Janda and A.B.P. Lever, *Inorg. Chem.* **31** (1992), p. 5172.
[71] R.K. Shervedani, M. Bagherzadeh and S.A. Mozaffari, *Sens. Actuators B* **115** (2006), p. 614.
[72] E. Katz and I. Wilner In: V.M. Mirsky, Editor, *Ultrathin Electrochemical Chemo- and Biosensors. Technology and Performance*, Springer-Verlag, New York (2004), p. 68 (Chapter 4).
[73] D.D. MacDonald, *Electrochim. Acta* **51** (2006), p. 1376.
[74] L. Yang and Y. Li, *Biosens. Bioelectron.* **20** (2005), p. 1407.
[75] R. de Cassia Silva Luz, F.S. Damos, A.B. de Oliviera, J. Beck and L.T. Kubota, *Electrochim. Acta* **50** (2005), p. 2675.
[76] H.O. Finklea and D.D. Hanshew, *J. Am. Chem. Soc.* **114** (1992), p. 3174.
[77] C.E.D. Chidsey, C.R. Bertozzi, T.M. Putvinski and A.M. Mujsce, *J. Am. Chem. Soc.* **112** (1990), p. 4301.
[78] C.E.D. Chidsey, *Science* **251** (1991), p. 919.

Corresponding author. Tel.: +27 12 4202515; fax: +27 12 3625297.
[1] ISE member